

Article

Synthesis, Characterization and Photophysical Properties of Mixed Ligand (η^3 -Allyl)palladium(II) Complexes with N,N' Aromatic Diimines

 Antonia Garypidou ¹, Konstantinos Ypsilantis ¹, Evaggelia Sifnaiou ¹, Maria Manthou ¹, Dimitris Thomos ¹, John C. Plakatouras ^{1,2}, Theodoros Tsolis ¹ and Achilleas Garoufis ^{1,2,*}

¹ Department of Chemistry, University of Ioannina, GR-45110 Ioannina, Greece; a.garypidou@uoi.gr (A.G.); k_ypsilantis@yahoo.gr (K.Y.); e.sifnaiou@uoi.gr (E.S.); maria.manthou13@gmail.com (M.M.); d.thomos@uoi.gr (D.T.); iplakatu@uoi.gr (J.C.P.); t.tsolis@uoi.gr (T.T.)

² Institute of Materials Science and Computing, University Research Center of Ioannina (URCI), GR-45110 Ioannina, Greece

* Correspondence: agaroufi@uoi.gr

Abstract: Palladium(II) complexes of the general formula $[\text{Pd}(\eta^3\text{-C}_3\text{H}_5)(\text{L})](\text{PF}_6)$, where L is 4,7-diphenyl-1,10-phenanthroline (**1**), 2,9-dimethyl-1,10-phenanthroline (**2**), 2,9-dimethyl-4,7-diphenyl-1,10-phenanthroline (**3**), 5-methyl-1,10-phenanthroline (**4**), 3,4,7,8-tetramethyl-1,10-phenanthroline (**5**), and 2-(2'-pyridyl) quinoxaline (**6**), were synthesized and characterized using high-resolution ESI-MS, NMR techniques and, in the case of (**6**), single-crystal X-ray diffraction methods. In addition, their photophysical properties were investigated. Complexes (**1**)–(**6**) were emitted in the greenish-blue region, with those containing methyl-substituted phenanthrolines having the higher quantum yield ($\approx 14\%$) in the solid state.

Keywords: (η^3 -allyl)palladium(II); metal complexes; emission spectra; phenanthrolines



Citation: Garypidou, A.; Ypsilantis, K.; Sifnaiou, E.; Manthou, M.; Thomos, D.; Plakatouras, J.C.; Tsolis, T.; Garoufis, A. Synthesis, Characterization and Photophysical Properties of Mixed Ligand (η^3 -Allyl)palladium(II) Complexes with N,N' Aromatic Diimines. *Chemistry* **2023**, *5*, 2476–2489. <https://doi.org/10.3390/chemistry5040162>

Received: 23 October 2023

Revised: 9 November 2023

Accepted: 9 November 2023

Published: 12 November 2023



Copyright: © 2023 by the authors. Licensee MDPI, Basel, Switzerland. This article is an open access article distributed under the terms and conditions of the Creative Commons Attribution (CC BY) license (<https://creativecommons.org/licenses/by/4.0/>).

1. Introduction

In recent years, much research has focused on the synthesis of luminescent compounds, owing to their application in various fields, such as lightemitting devices (OLEDs) [1–4], image biomarkers [5–8], photodynamic therapy [9] and others [10–13].

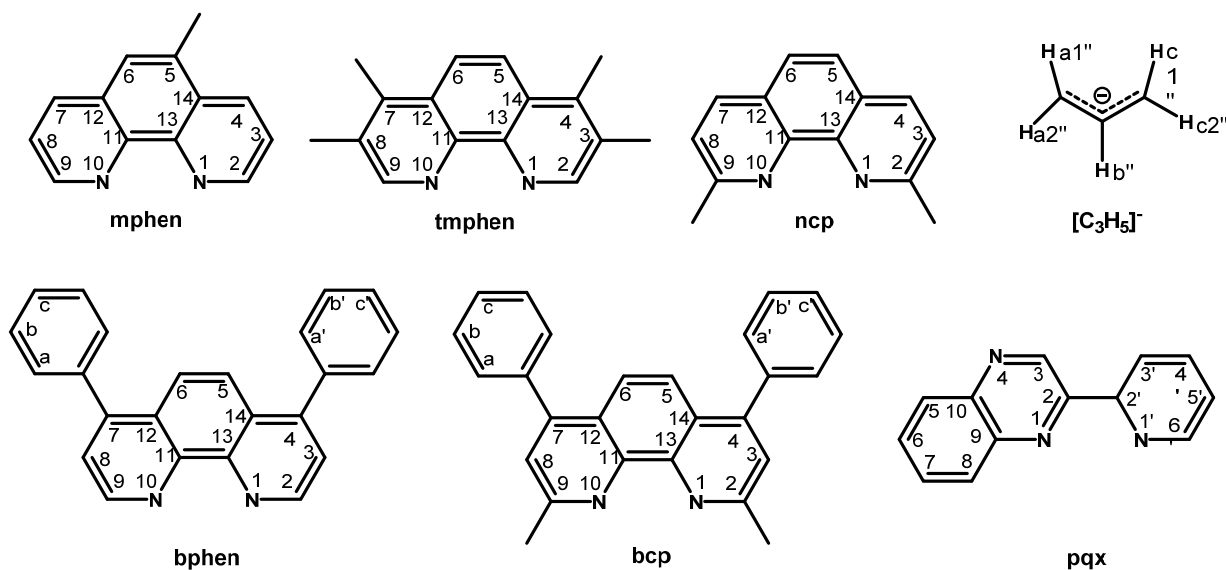
Organometallic compounds have been studied extensively due to their advantages over their organic ligands, primarily stemming from the metal center [14]. The higher the spin-orbit coupling (SOC) constant of the transition metal, the greater the potential for intersystem crossing, leading to enhanced exciton harvesting in the T1 triplet state and, consequently, increased emission intensity [15]. Notably, compounds containing metal ions from the second and third transition rows tend to exhibit greater emissivity due to the higher overlap of their 4d or 5d orbitals with the orbitals of the ligand [16]. Among the well-established efficient triplet emitters are complexes of platinum [17–21], ruthenium [22,23] and iridium [23,24]. However, the recent literature reports studies involving palladium(II) complexes with luminescent properties [14]. The current data are not particularly encouraging, as only a few Pd(II) complexes exhibit luminescence. This is attributed to both the weak SOC effect and the presence of thermally accessible metal-centered (MC) d-d* states, resulting in distortion of the excited state structure and efficient non-radiative decay [25,26]. Notably, orthometalated Pd(II) complexes have received significant attention, with several demonstrating luminescent properties, where the presence of the metal enhances the emission in comparison with that of the free ligand [27–30]. Consequently, the exploration of the photophysical properties of Pd(II) complexes remains a relatively unexplored, yet intriguing, field of research.

In addition to the transition metal, the nature of ligands plays an important role in the photophysical properties of organometallic compounds. Complexes containing chelating

ligands with carbon and nitrogen donor atoms have been extensively reported in the relevant literature [14]. Specifically, complexes of 1,10-phenanthroline derivatives have been reported to exhibit attractive luminescence features [31]. Recently, de Franca et al. synthesized a complex of Pd(II) with 1,10-phenanthroline, achieving a remarkable quantum yield of over 50% [32]. Furthermore, a binuclear complex of Pd(II) with a bis-*N,N'* chelating bridging perylene diimide ditopic ligand, while displaying a low quantum yield, exhibited a higher quantum yield than the free ligand [33].

Although allyl is a common anionic ligand in organometallic chemistry, mixed ligand complexes with phenanthroline-like *N,N'* chelating ligands have rarely been reported in the literature [34–38]. In general, complexes with the η^3 -allyl-Pd(II) moiety have been investigated for their applications in catalytic processes [39–41] and their cytotoxic activity [42–45]. However, only a few reports deal with the examination of such type complexes regarding their photophysical features. Mayoral et al. reported that two compounds of [Pd(η^3 -allyl)] with β -diketone derivatives exhibited luminescent properties [46]. More recently, allyl palladium complexes bearing imidazo[1,5-a]pyridino-3-ylidene and dipyrroimidazolinylidene ligands have been synthesized and studied for their photophysical properties. The results demonstrated that these organometallic compounds exhibit luminescent characteristics, with the Φ value reaching up to 0.20 [47].

In this study, we synthesized and characterized six novel allyl palladium organometallic complexes (1)–(5), containing substituted 1,10-phenanthrolines and (6) containing 2-(2'-pyridyl)quinoxaline as *N,N'* chelating ligands (Scheme 1). In addition, we investigated their photophysical properties and examined how the nature of the chelating ligand affects the fluorescence of the complexes.



Scheme 1. Structures and numbering of ligands used in this study. mphen = 5-methyl-1,10-phenanthroline, tmphen = 3,4,7,8-tetramethyl-1,10-phenanthroline, ncp = 2,9-dimethyl-1,10-phenanthroline, bphen = 4,7-diphenyl-1,10-phenanthroline, bcp = 2,9-dimethyl-4,7-diphenyl-1,10-phenanthroline and pqx = 2-(2'-pyridyl)quinoxaline.

2. Experimental

2.1. Materials and Methods

All solvents and chemicals were analytical grade and were used without further purification. Sodium tetrachloridopalladate(II) (99.9%) and 3-chloro-1-propene were purchased from Alfa Aesar. 2-acetyl-pyridine (99.0%) was purchased from Merck Chemical Company. The ligands 4,7-Diphenyl-1,10-phenanthroline (bphen), 2,9-Dimethyl-1,10-phenanthroline (ncp), 2,9-Dimethyl-4,7-diphenyl-1,10-phenanthroline (bcp), 5-Methyl-1,10-phenanthroline (mphen), and 3,4,7,8-Tetramethyl-1,10-phenanthroline (tmphen) were purchased from

Sigma Aldrich. 2-(2'-pyridyl)quinoxaline (pqx) was synthesized according to the literature [48]. High-resolution electrospray ionization mass spectra (HR-ESI-MS) were obtained on a Thermo Scientific, LTQ Orbitrap XL™ system. C, H, and N determinations were performed on a Perkin-Elmer 2400 Series II analyzer. ¹H NMR spectra were recorded on Bruker Avance NEO and Avance II spectrometers operating at proton frequencies of 400.13 and 500.13 MHz, while ¹³C at frequency 125 MHz, and processed using Topspin 4.07 (Bruker Analytik GmbH). Two-dimensional COSY, TOCSY, and NOESY spectra were recorded following standard Bruker procedures. NOESY spectra were recorded in mixing times in the range from 600 to 800 ms. The UV-Vis spectra of the complexes were recorded on Agilent Cary 60 UV-Vis Spectrophotometer with xenon source lamp, in solution of CH₂Cl₂ and in solid state. The fluorescence emission study was carried out using a Jasco FP-8300 fluorometer equipped with a xenon lamp source. The luminescence quantum yields of the solutions (C = 1 × 10⁻⁴ M) were determined using the equation $Q_s = Q_r(A_r/A_s)(E_s/E_r)(n_s/n_r)^2$, using [Ru(bpy)₃]Cl₂ in air-equilibrated water solution as a reference standard (Q_r = 0.04). 'A' stands for the absorbance of the solution, 'E' for the integrated fluorescence intensity of the emitted light, 'n' is the refractive index of the solvents and subscripts 'r' and 's' correspond to the reference and the sample, respectively. Using the equation $Q = S_2/S_0 - S_1$, the quantum yields of the solid state of the complexes were calculated. S₂ denotes the integrated emission intensity of the sample and S₀, S₁ stand for the excitation intensities of the standard and the sample, respectively.

2.2. Synthesis of the Complexes

Complexes (1)–(6) were synthesized in a similar manner. In a typical procedure, 0.20 mmol of the ligand was added to a stirred solution of CH₂Cl₂ (10 mL) containing 0.05 mmol of the dimer [Pd(η³-C₃H₅)Cl]₂ at room temperature, according to the literature [49] (Figures S1 and S2, in the Supplementary Materials). The reaction mixture was stirred for 2 h, and a pale-yellow precipitate appeared. It was collected with centrifugation, washed twice with 5 mL of CH₂Cl₂, and dissolved in 10 mL of acetone. An aqueous solution (20 mL) containing 1 mmol of NH₄PF₆ was added slowly, and the mixture was kept at 4 °C overnight. A microcrystalline yellow precipitate was collected, washed with 5 mL of H₂O, and dried under vacuum.

[Pd(η³-C₃H₅)(bphen)]PF₆ (1): Yield: 75%. C₂₇H₂₁F₆N₂PPd: calc.% C, 51.9; H, 3.39; N, 4.48; found C, 51.6; H, 3.41; N, 4.49. HR-ESI-MS, positive (*m/z*): found 479.0743 calc. 479.0743 for [C₂₇H₂₁N₂Pd]⁺. ¹H NMR: (500 MHz, 298 K, acetone-d₆, δ in ppm), H_{2/9} 9.57, (d, 2H), H_{3/8} 8.18, (d, 2H), H_{5/6} 8.27, (s, 2H), H_{a/b/c} 7.76, (m, 10H), H_{a1''/c1''} 4.78, (d, 2H), H_{b''} 6.34, (m, 1H), H_{a2''/c2''} 3.90, (d, 2H).

[Pd(η³-C₃H₅)(ncp)]PF₆ (2): Yield: 82%. C₁₇F₆H₁₇N₂PPd: calc.% C, 40.78; H, 3.42; N, 5.59; found C, 40.82; H, 3.40; N, 5.57. HR-ESI-MS, positive (*m/z*): found 355.0425 calc. 355.0421 for [C₁₇H₁₇N₂Pd]⁺. ¹H NMR: (500 MHz, 298 K, acetone-d₆, δ in ppm), H_{4/7} 8.76, (d, 2H), H_{3/8} 8.04, (d, 2H), H_{5/6} 8.15, (d, 2H), H_{CH3} 3.10, (s, 6H), H_{a1''/c1''} 4.90, (d, 2H), H_{b''} 5.91, (m, 1H), H_{a2''/c2''} 3.80, (d, 2H).

[Pd(η³-C₃H₅)(bcp)]PF₆ (3): Yield: 87%. C₂₉H₂₅F₆N₂PPd: calc.% C, 53.35; H, 3.86; N, 4.29; found C, 53.30; H, 3.89; N, 4.31. HR-ESI-MS, positive (*m/z*): found 507.1065 calc. 507.1047 for [C₂₉H₂₅N₂Pd]⁺. ¹H NMR: (500 MHz, 298 K, acetone-d₆, δ in ppm), H_{3/8} 8.08, (s, 2H), H_{5/6} 8.08, (s, 2H), H_{aa'/bb'/cc'} 7.69, (m, 10H), H_{a1''/c1''} 4.99, (d, 2H), H_{b''} 6.03, (m, 1H), H_{a2''/c2''} 3.87, (d, 2H), H_{CH3} 3.24, (s, 6H).

[Pd(η³-C₃H₅)(mphen)]PF₆ (4): Yield: 91%. C₁₆H₁₅F₆N₂PPd: calc.% C, 39.49; H, 3.11; N, 5.76; found C, 39.53; H, 3.09; N, 5.74. HR-ESI-MS, positive (*m/z*): found 341.0274 calc. 341.0265 for [C₁₆H₁₅N₂Pd]⁺. ¹H NMR: (500 MHz, 298 K, acetone-d₆, δ in ppm), H_{3/8} 8.14, (m, 2H), H₂ 9.45, (d, 1H), H₄ 9.09, (d, 1H), H₆ 8.20, (t, 1H), H₇ 8.88, (d, 1H), H₉ 9.36, (d, 1H), H_{a1''/c1''} 4.67, (d, 2H), H_{b''} 6.24, (m, 1H), H_{a2''/c2''} 3.70, (d, 2H), H_{CH3} 2.94 (s, 3H). ¹³C NMR: (125 MHz, 298 K, acetone-d₆, δ in ppm) C_{9/2} 155.3/154.8, C_{11/13} 146.0/146.1, C_{7/4} 140.1/138.1, C₅ 136.7, C_{12/14} 131.6/131.2, C_{3/8} 127.5/127.4, C₆ 127.2, C_(CH3) 18.8, C_b 121.2, C_{a/c} 63.3/63.0.

[Pd(η^3 -C₃H₅)(tmphen)]PF₆ (5): Yield: 79%. C₁₉H₂₁F₆N₂PPd: calc.% C, 43.16; H, 4.00; N, 5.30; found C, 43.10; H, 3.13; N, 5.76. HR-ESI-MS, positive (*m/z*): found 383.0742 calc. 383.0734 for [C₁₉H₂₁N₂Pd]⁺. ¹H NMR: (500 MHz, 298 K, acetone-d₆, δ in ppm), H_{2/9} 9.29, (s, 2H), H_{5/6} 8.47, (s, 2H), H_{a1''/c1''} 4.63, (d, 2H), H_{b''} 6.19, (m, 1H), H_{a2''/c2''} 3.73, (d, 2H), H_{CH3} 2.91 (s, 6H), H_{CH3} 2.68 (s, 6H). ¹³C NMR: (125 MHz, 298 K, acetone-d₆, δ in ppm), C_{2/9} 156.1, C_{11/13} 148.7, C_{5/6} 124.5, C_{3/8} 136.1, C_{4/7} 129.7, C_{12/14} 145.3, C_{(3/8)CH3} 17.5, C_{(4/7)CH3} 15.3, C_b 120.7, C_{a/c} 62.7.

[Pd(η^3 -C₃H₅)(pqx)]PF₆ (6): Yield: 82%. C₁₆H₁₄F₆N₃PPd: calc.% C, 40.66; H, 4.17; N, 7.90; found C, 40.70; H, 4.16; N, 7.87. HR-ESI-MS, positive (*m/z*): found. 354.0224 calc. 354.0217 for [C₁₆H₁₄N₃Pd]⁺. ¹H NMR: (500 MHz, 298 K, acetone-d₆, δ in ppm), H₅ 8.55, (d, 1H), H_{4'} 8.61(t, 1H), H_{6/7} 8.21, (m, 2H), H₃ 10.25, (s, 1H), H_{6'} 9.30, (d,1H), H_{3'}9.16, (d, 1H), H₈ 8.40, (d, 1H), H_{5'} 8.06, (t, 1H), H_{a1''/c1''} 5.02, (d, 2H), H_{b''} 6.30, (m, 1H), H_{a2''/c2''} 4.08, (d, 2H). Suitable bright-yellow crystals of (6), for X-ray analysis, were grown from an aqueous acetone solution containing dissolved solids initially isolated from the reaction mixture in the presence of NH₄PF₆ in the fridge. However, crystals of (6a) were obtained from the reaction mixture layered with diethyl ether and characterized with ¹H and ¹³C NMR. Pd(η^3 -C₃H₅)(pqx) [Pd(η^3 -C₃H₅)Cl₂] (6a): ¹H NMR: (500 MHz, 298 K, methanol-d₄, δ in ppm), [Pd(η^3 -C₃H₅)(pqx)]⁺: H₅ 8.43, (d, 1H), H_{4'} 8.44(t, 1H), H_{6/7} 8.13, (m, 2H), H₃ 10.08, (s, 1H), H_{6'} 8.94, (d, 1H), H_{3'} 9.12, (d, 1H), H₈ 8.39, (d, 1H), H_{5'} 7.90, (t, 1H), H_{a1''/c1''} 4.87, (d, 2H), H_{b''} 6.18, (m, 1H), H_{a2''/c2''} 3.93, (d, 2H). [Pd(η^3 -C₃H₅)Cl₂]⁻: H_{a1''/c1''} 4.05, (d, 2H), H_{b''} 5.58, (m, 1H), H_{a2''/c2''} 3.03, (d, 2H). ¹³C NMR: (125 MHz, 298 K, methanol-d₄, δ in ppm) [Pd(η^3 -C₃H₅)(pqx)]⁺: C₂ 151.7, C₃ 146.0, C_{2'} 155.3, C_{3'} 126.7, C_{4'} 130.1, C_{5'} 142.3, C_{6'} 156.0, C₉ 146.0, C₁₀ 142.3, C_{5/8} 131.6/131.1, C_{6/7} 134.6/134.1, C_b 120.5, C_{a/c} 62.6. [Pd(η^3 -C₃H₅)Cl₂]⁻: C_b 112.8, C_{a/c} 65.9.

2.3. Crystal Structure Determinations

Suitable crystals were glued to a thin glass fiber with cyanoacrylate (super glue) adhesive and placed on the goniometer head. Diffraction data were collected on a Bruker D8 Quest Eco diffractometer, equipped with a Photon II detector and a TRIUMPH (curved graphite) monochromator utilizing Mo K α radiation ($\lambda = 0.71073 \text{ \AA}$) using the APEX 3 software package [50]. The collected frames were integrated with the Bruker SAINT software using a wide-frame algorithm. Data were corrected for absorption effects using the Multi-Scan method (SADABS) [51]. The structures were solved using the Bruker SHELXT Software Package and refined by full-matrix least squares techniques on F² (SHELXL 2018/3) [52] via the ShelXle interface [53]. The non-H atoms were treated anisotropically, whereas the organic H atoms were placed in calculated, ideal positions and refined as riding on their respective carbon atoms. PLATON [54] was used for geometric calculations, and X-Seed [55] for molecular graphics. Details on data collection and refinement are presented in Table 1. Full details on the structures can be found in the CIF files in the ESI. CCDC 2301621 and 2301622 contain the supplementary crystallographic data for this paper. These data can be obtained free of charge via www.ccdc.cam.ac.uk/data_request/cif.

Table 1. Crystal data and structural refinement for compounds [Pd(η^3 -C₃H₅)(pqx)]PF₆ (6) and [Pd(η^3 -C₃H₅)(pqx)][Pd(η^3 -C₃H₅)Cl₂] (6a).

Compound	(6)	(6a)
Empirical formula	C ₁₆ H ₁₄ F ₆ N ₃ PPd	C ₁₉ H ₁₉ Cl ₂ N ₃ Pd ₂
Formula weight	499.67	573.12
Temperature (K)	296(2)	
Wavelength (\AA)	0.71073	
Crystal system	Orthorhombic	Monoclinic

Table 1. Cont.

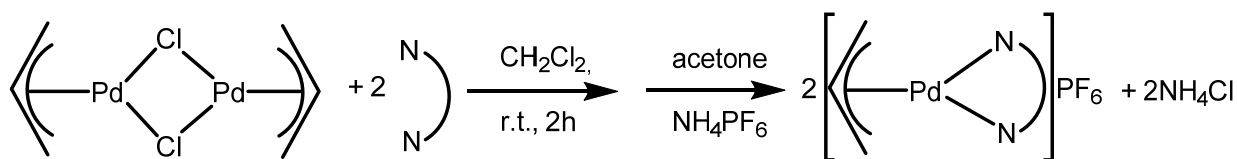
Compound	(6)	(6a)
Space group	<i>Pnma</i>	<i>P2₁/c</i>
Unit cell dimensions a, b, c (Å), α, β, γ (°)	18.7765(10), 6.8527(3), 16.4449(10), 90, 90, 90	6.9296(3), 29.3104(12), 9.8311(5), 90, 98.680(2), 90
Volume (Å ³)	2115.96(19)	1973.92(15)
Z	4	4
Density (calcd.) (g/cm ³)	1.569	1.928
Absorption coefficient (mm ⁻¹)	1.008	2.100
F(000)	984	1120
Crystal size (mm ³)	0.600 × 0.120 × 0.080	0.500 × 0.040 × 0.040
θ range for data collection (°)	2.477 to 24.996	2.780 to 24.991
Index ranges	−22 ≤ h ≤ 22, −8 ≤ k ≤ 7, −19 ≤ l ≤ 19	−8 ≤ h ≤ 7, −34 ≤ k ≤ 34, −11 ≤ l ≤ 11
Reflections collected	34567	44871
Independent reflections	2031 [R _{int} = 0.0499]	3452 [R _{int} = 0.0801]
Completeness to θ = 24.996°	99.8%	99.2%
Refinement method	Full-matrix least-squares on F ²	
Data/restraints/parameters	2031/0/158	3452/180/291
Goodness-of-fit	1.185	1.239
Final R indices [I > 2σ(I)]	R _{obs} = 0.0405, wR _{obs} = 0.1089	R _{obs} = 0.0834, wR _{obs} = 0.1664
R indices [all data]	R _{all} = 0.0439, wR _{all} = 0.1110	R _{all} = 0.0947, wR _{all} = 0.1699
Largest diff. peak and hole (e·Å ⁻³)	0.452 and −1.135	1.703 and −1.761

$R = \sum ||F_o| - |F_c|| / \sum |F_o|$, $wR = \{\sum [w(|F_o|^2 - |F_c|^2)^2] / \sum [w(|F_o|^4)]\}^{1/2}$ and $w = 1 / [\sigma^2(F_o^2) + (aP)^2 + bP]$ where $p = (F_o^2 + 2F_c^2) / 3$ where for **6**: a = 0.0527, b = 3.6386; **6a**: a = 0, b = 49.5689.

3. Results and Discussion

3.1. Synthesis and Characterization of Complexes (1)–(6)

Complexes (1)–(6) were formed from the reaction of the dimer [Pd(η^3 -C₃H₅)Cl]₂ with the chelating ligand N,N', in a non-coordinative solvent, such as CH₂Cl₂ and subsequently isolated as [PF₆][−] salts, according to Scheme 2 as follows:



Scheme 2. Synthetic procedure for complexes (1)–(6).

The ¹H NMR spectra of complexes (1)–(6) in acetone exhibit, in addition to signals corresponding to the aromatic protons, three signals attributed to the η^3 -allyl protons. These signals include a one-proton multiplet, ranging from 5.91 to 6.34 ppm, assigned to Hb'', a two-proton doublet ranging from 4.67 to 5.02 ppm with a ³J coupling constant of 6.5–7.5 Hz, assigned to Ha2''/Hc2'' *syn* to Hb'' and another two-proton doublet, ranging from 3.70 to 4.08 ppm with ³J = 13.5–14.5 Hz, assigned to Ha1''/Hc1'' *anti* to Hb'' (Figure 1).

The distinction between the doublets of Ha2''/Hc2'' and Ha1''/Hc1'' was made based on the general principle that the ³J value for *trans*-protons in a double bond C-C is lower than that for the corresponding *cis*-protons [47]. Moreover, in the 600 ms NOESY spectrum of (2), we observe a cross-peak, opposite to diagonal, between the ncp methyl groups and

the signal assigned to Ha1''/Hc1''. This indicates a proximity between these protons. Also, all the NOE connectivities between the η^3 -allyl protons were observed (Figure 2).

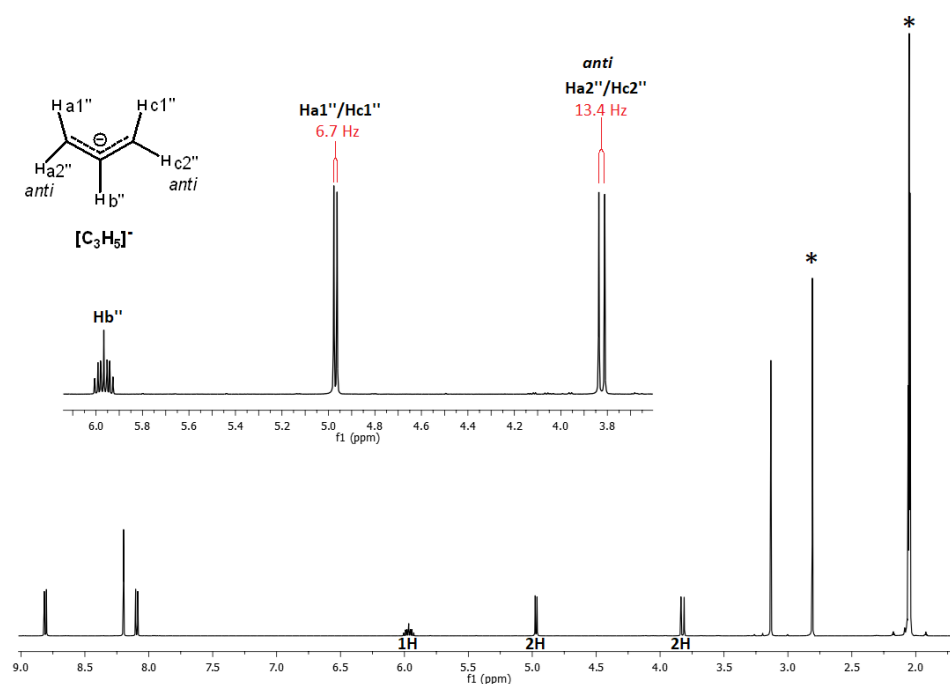


Figure 1. ^1H NMR spectrum of complex (2) in acetone- d_6 . Inset shows the expansion of the spectrum aliphatic area and the numbered structure of the η^3 -allyl anionic ligand. Peaks with asterisk denote the solvent and the HOD.

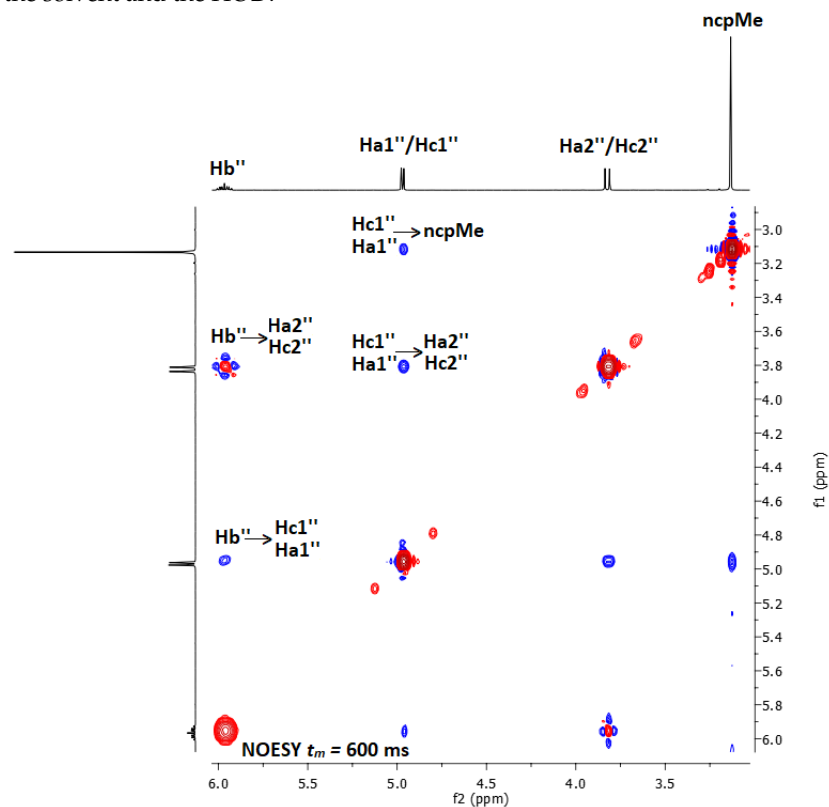


Figure 2. The NOESY spectrum of (2) at mixing time 600 ms, in acetone- d_6 at 298 K showing the NOE connectivities between the η^3 -allyl protons and between the methyl groups of ncp and the allyl *syn* protons, Hc1''/Ha1''.

The chemical shifts of Hb'' appear to be affected by the intrinsic basicity of the chelated phenanthroline. In general, the methyl-substituted phenanthrolines are stronger bases than the phenanthroline itself, which, however, is stronger base than its phenyl-substituted derivatives. Thus, the deshielding effect on Hb'' is more pronounced as the pKa of the chelated phenanthroline decreases. For instance, 2,9-dimethyl-1,10-phenanthroline [56] (pKa = 6.15 and δ = 5.91 ppm); 5-methyl-1,10-phenanthroline [56] (pKa = 5.2 and δ = 6.24 ppm) > 1,10-phenanthroline [57] (pKa = 4.92 and δ = 6.30 ppm) > 4,7-diphenyl-1,10-phenanthroline [58] (pKa = 4.55 and δ = 6.34 ppm). With respect to the chelated ligand, the protons at neighboring sites of the coordinated nitrogen atoms shifted downfield, as expected, in the range of 0.26 to 0.47 ppm (Figures S3–S8, in the Supplementary Materials). The ^{13}C NMR spectra of the complexes (4), (5) and (6a) are presented in Figures S15–S17 (in the Supplementary Materials).

In the HR-ESI-MS of complexes (1)–(6), only one cluster peak assignable to the positive single-charged cation $[\text{Pd}(\eta^3\text{-C}_3\text{H}_5)(\text{L})]^+$ was observed (S9–S14).

3.2. Crystal Structures of $[\text{Pd}(\eta^3\text{-C}_3\text{H}_5)(\text{pqx})]\text{PF}_6$ (6) and $[\text{Pd}(\eta^3\text{-C}_3\text{H}_5)(\text{pqx})][\text{Pd}(\eta^3\text{-C}_3\text{H}_5)\text{Cl}_2]$ (6a)

Suitable crystals for X-ray diffraction studies of (6) were grown from an aqueous acetone solution containing dissolved solids initially isolated from the reaction mixture in presence of NH_4PF_6 in the fridge, while crystals of (6a) were isolated by layering the reaction mixture with diethyl ether. The same procedure to obtain crystals for complexes (1)–(5) was followed without success. Selected bond lengths and angles for both compounds are presented in Table 2.

Table 2. Selected bond distances (Å) and angles (°) for $[\text{Pd}(\eta^3\text{-C}_3\text{H}_5)(\text{pqx})]\text{PF}_6$ (6) and $[\text{Pd}(\eta^3\text{-C}_3\text{H}_5)(\text{pqx})][\text{Pd}(\eta^3\text{-C}_3\text{H}_5)\text{Cl}_2]$ (6a).

Compound (6)			
Pd(1)–N(1)	2.144(4)	Pd(1)–N(3)	2.090(5)
Pd(1)–C(1A)	2.150(6)	Pd(1)–C(2A)	2.137(7)
Pd(1)–C(3A)	2.115(5)		
N(1)–Pd(1)–C(1A)	111.71(18)	N(1)–Pd(1)–N(3)	78.19(19)
N(1)–Pd(1)–C(2A)	142.7(2)	N(1)–Pd(1)–C(3A)	179.63(19)
N(3)–Pd(1)–C(1A)	170.11(19)	N(3)–Pd(1)–C(3A)	102.2(2)
N(3)–Pd(1)–C(2A)	132.66(18)	C(1A)–Pd(1)–C(3A)	67.93(13)
Compound (6a)			
Pd(1)–N(1)	2.170(9)	Pd(1)–N(3)	2.082(11)
Pd(1)–C(1A)	2.13(12)	Pd(1)–C(2A)	2.18(8)
Pd(1)–C(3A)	2.17(12)	Pd(2)–C(1B)	2.07(6)
Pd(2)–Cl(1)	2.369(4)	Pd(2)–C(2B)	2.11(3)
Pd(2)–Cl(2)	2.381(4)	Pd(2)–C(3B)	2.07(5)
N(1)–Pd(1)–C(1A)	167(3)	N(1)–Pd(1)–N(3)	78.0(4)
N(1)–Pd(1)–C(2A)	141(2)	N(1)–Pd(1)–C(3A)	117(3)
N(3)–Pd(1)–C(1A)	93(3)	N(3)–Pd(1)–C(3A)	163(3)
N(3)–Pd(1)–C(2A)	134(2)	C(1A)–Pd(1)–C(3A)	74(4)
Cl(1)–Pd(2)–Cl(2)	95.82(16)	C(1B)–Pd(2)–Cl(1)	96.5(15)
C(2B)–Pd(2)–Cl(1)	127.1(9)	C(3B)–Pd(2)–Cl(1)	169.1(10)
C(1B)–Pd(2)–Cl(2)	166.6(16)	C(2B)–Pd(2)–Cl(2)	133.8(9)
C(3B)–Pd(2)–Cl(2)	95.1(10)		

Compound (6) crystallizes in the orthorhombic space group $Pnma$ with its asymmetric unit containing halves of the cation $[\text{Pd}(\eta^3\text{-C}_3\text{H}_5)(\text{pqx})]^+$ and the anion PF_6^- lying on a mirror plane. All the atoms of the cation, except for the central allyl carbon atom, are on that mirror plane and its structure is presented in Figure 3. The palladium atom is formally five-coordinated, since the allyl ligand utilizes all its carbon atoms for coordination, adopting a η^3 -binding mode. Though, ignoring the coordination of C(2A), the coordination sphere of Pd(1) can be considered as distorted square planar. The planarity of the coordination sphere

is imposed by the above-mentioned mirror plane, but the *cis* coordination sphere angles deviate significantly from 90° . This is due to the small bite angle of the pqx ligand and to the even smaller C(1A)–Pd(1)–C(3A) allyl angle. The Pd–N and Pd–C bond distances agree with literature values for similar complexes. (See, for example, Refs [59–61]).

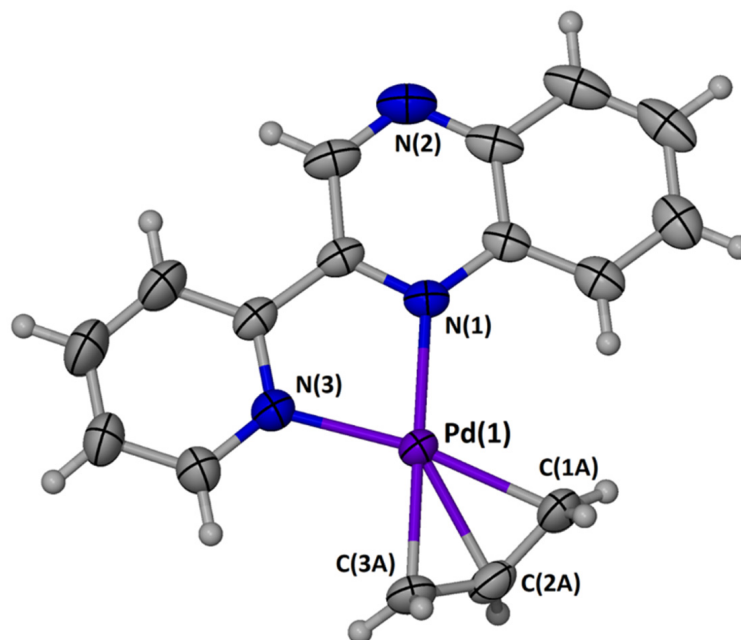


Figure 3. A partially labeled thermal ellipsoid plot (50% probability level) of the cation in the crystal structure of (6). Only one part of the disordered allyl group is shown for clarity.

There is a small difference between the Pd–N bond distances, reflecting the expected difference based on the basicity of pyridine and quinoxaline nitrogen atoms. Although the C(1A) and C(3A) atoms of the allyl group are on the mirror plane hosting the coordination sphere, C(2A) is disordered in two positions, above and below the plane, as imposed by the symmetry. The dihedral angle between the coordination sphere plane and the allyl plane is 67.2° . The geometrical characteristics of the allyl group deviate slightly from the ideal values, with the mean C–C distance and C–C–C angle being respectively 1.38 \AA and 119.4° (ideal values: ca. 1.36 \AA and 120° , respectively). The small difference between the Pd–C(1A) and Pd–C(3A) bond distances is related to the different *trans* influence of the N atoms of the heterocyclic ligand.

Symmetry-related ($-x+1, y-1/2, -z+1$) complex cations interact with π – π stacking interactions via the quinoxaline moiety, forming positively charged columns parallel to the *b*-axis of the unit cell. The characteristics of the interaction are: centroid distance, 3.90 ; least-square plane distance, 3.43 ; centroid offset, 1.86 \AA . The counter anions are located between the columns interacting with non-conventional C–H \cdots F H-bonds. A packing diagram is shown in Figure S18.

In absence of other counter anions (i.e., PF_6^-) from the reaction system, compound (6a) can be isolated. It crystallizes in the monoclinic space group $P2_1/c$ and consists of ionic pairs $[\text{Pd}(\eta^3\text{-C}_3\text{H}_5)(\text{pqx})][\text{Pd}(\eta^3\text{-C}_3\text{H}_5)\text{Cl}_2]$ interacting with each other in the lattice via stacking interactions and non-conventional C–H \cdots Cl H-bonds. A view of the ionic pair is shown in Figure 4. Despite the lowered accuracy of the bond lengths and angles in the structure of (6a), due to the disordered allyl groups, the structural characteristics, and the observations of the differences between the Pd–N and Pd–C bond lengths and angles are very similar to (6) and will not be described in detail.

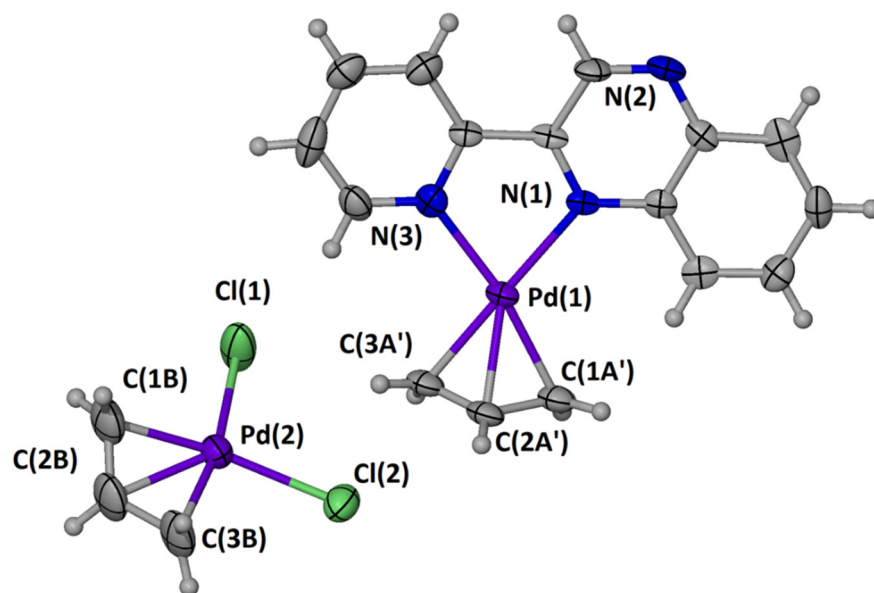


Figure 4. A partially labeled thermal ellipsoid plot (50% probability level) of the ionic pair in the crystal structure of (6a). Only the parts with the highest occupancy of the disordered allyl groups are shown for clarity.

To our surprise, ionic pairs containing palladiumallyl complexes in both cations and anions are scarce in the literature. Compound (6a) is the ninth member of this family [62] (CSD codes: AQICOS, AQICUY, BEHMIK, HAJKAE, IZIXIB, OZUHUN, OZUJAV, QOH-PUZ). The structural characteristics of the anion are consistent within the observed values. (See for example, [63–65]).

In the lattice, the cations are arranged in a similar fashion as in (6), forming columns, but the stacking interactions of symmetry related $(-x+2, -y+1, -z+1)$ quinoxaline moieties lead to the formation of stacked dimers. The characteristics of the interaction are centroid distance, 3.77; least-square plane distance, 3.39; centroid offset, 1.65 Å. The counter anions are located between the columns interacting with non-conventional C–H \cdots Cl H-bonds. A packing diagram is shown in Figure S19.

3.3. Photophysical Properties of Complexes (1)–(6)

The photophysical data of complexes (1)–(6) are summarized in Table 3. Solid state absorption and emission spectra are presented in Figure 5, while the corresponding solution spectra are presented in Figure 6.

Table 3. Photophysical data of complexes (1)–(6) in solid state and CH₂Cl₂-diluted solutions. Excitation in solid state, $\lambda_{exc} = 400$ nm and in CH₂Cl₂, $\lambda_{exc} = 365$ nm.

Complex	UV/Vis Absorbance λ_{max} (nm), ($\epsilon \times 10^4$ M ⁻¹ cm ⁻¹)		Emission λ_{em} (nm)		QY (%)	
	Solid	Solution	Solid	Solution	Solid	Solution
(1) bp	237, 309, 420	232(18), 292(20), 321sh, 360(2)	478, 565	433	3%	1.6%
(2) ncp	238, 311, 394sh	234(40), 279(35), 295sh, 355(1)	477, 566	436	12.6%	1.2%
(3) bcp	239, 311, 370sh	233(41), 294(42), 359(2.5)	478, 565	433, 533sh	6%	1%
(4) mp	232, 310, 358sh	233(34), 277(24), 297sh, 362(1)	478, 566	437	14%	1.15%
(5) tmp	236, 312, 352sh	236(37), 281(37), 304sh, 338(4.5)	476, 565	456sh, 486, 510sh	14%	2.8%
(6) pqx	305, 394	254(20), 364(16)	480, 565	437	1.9%	0.15%

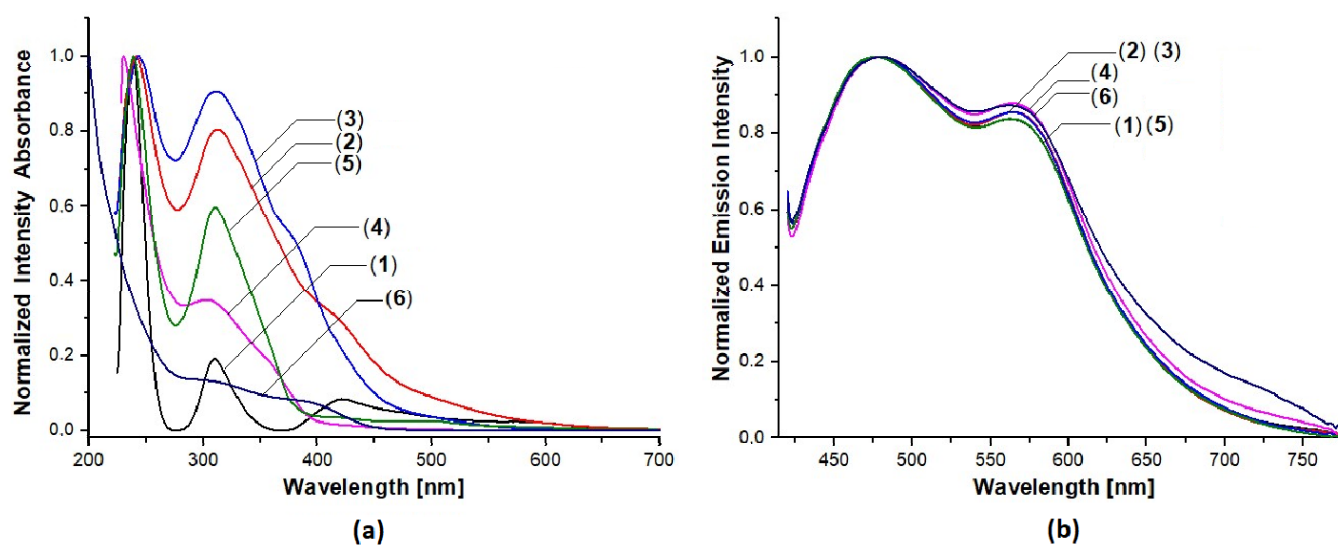


Figure 5. Solid state absorption (a) and emission (b) spectra of complexes (1)–(6).

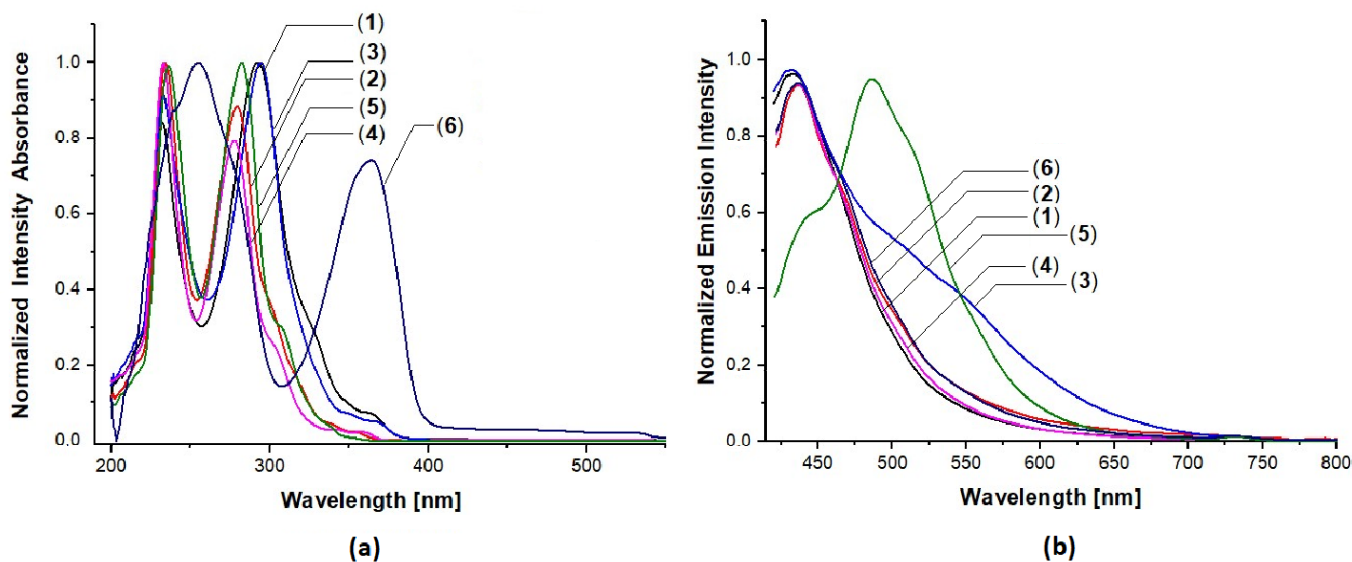


Figure 6. UV-Vis (a) and emission (b) spectra of complexes (1)–(6) in CH_2Cl_2 .

The solid-state UV-Vis spectra of compounds (1)–(6) (Figure 5) exhibit very similar bands below 350 nm, which are attributed to intraligand $\pi \rightarrow \pi^*$ transitions. The low energy absorption bands ranging from 352 to 420 nm probably arise from metal-to-ligand charge transfer (MLCT) transitions involving the N,N' -chelated ligands and the η^3 -allyl group. Upon excitation of the complexes at 400 nm, a greenish-blue emission centered at approximately 480 and 530 nm is observed for all the compounds. The quantum yield (QY) varies from 3 to 14%, depending on the nature of the chelated ligand. The complexes containing methyl-substituted phenanthrolines, (2), (4), and (5), exhibit significantly higher QYs compared to those with phenyl substitutions, (1) and (3). However, in diluted solutions of CH_2Cl_2 , lower QYs ranging from 1 to 2.8% were observed for all the complexes, (1)–(5). These results suggested that in solid-state the higher QYs arise from packing interactions, such as π -stacking, which are mainly favored by the presence of small substituents, like the methyl groups. In every case, the complexes exhibit higher QYs compared to that of the phenanthroline itself [31]. In similar platinum complexes with substituted phenanthrolines, the emission values solid state complexes are quite close to those of palladium, with the exception of the complex with bathophenanthroline, where a maximum of 620 nm

is observed. However, the quantum yields are very low, with some cases even falling below 1% [66].

The UV/Vis spectra of (1)–(6) in CH₂Cl₂ show similarities among complexes (1)–(5), involving strong intraligand $\pi \rightarrow \pi^*$ transitions below 350 nm and a weak intensity band ($\epsilon = 20\text{--}40 \times 10^4 \text{ M}^{-1}\text{cm}^{-1}$) at 348–362 nm, which is assigned to MLCT. In the case of Pt complexes with substituted phenanthrolines, the absorption spectra in CH₂Cl₂, show a spectral red-shift in comparison with the corresponding Pd ones, moving the λ_{max} of MLCT towards the visible region. Also, a similar phenomenon was observed in the emission spectra of Pt complex with bathophenanthroline ($\lambda_{\text{em}} = 600 \text{ nm}$) [66]. However, the spectrum of (6) significantly differs from those of (1)–(5), showing two similar intense bands ($\epsilon_{254} = 20 \times 10^4 \text{ M}^{-1}\text{cm}^{-1}$, $\epsilon_{364} = 16 \times 10^4 \text{ M}^{-1}\text{cm}^{-1}$) at 254 and 364 nm, probably reflecting the lower rigidity of ppx compared to the phenanthroline ring.

The emission spectra of complexes (1)–(4) and (6) are similar, with λ_{em} ranging from 433–437 nm and low QYs (0.15–1.6%). However, complex (5) exhibits an almost green emission, having the highest QY (2.8%) among all the studied complexes.

4. Conclusions

The reaction between the dimer [Pd(η^3 -C₃H₅)Cl]₂ and N,N' aromatic diimines (L) yielded mixed-ligand cationic complexes of the general formula [Pd(η^3 -C₃H₅)(L)]⁺. The complexes were isolated as [PF₆][−] salts and characterized using high-resolution ESI-MS, NMR spectroscopic techniques and X-ray single-crystal diffraction methods. It was observed that the chemical shift of the coordinated η^3 -allylHb" was affected by the intrinsic basicity of the chelated phenanthroline, reflecting the *trans* influence of the chelated ligand on the η^3 -coordinated allyl group. All the synthesized complexes emitted in the greenish-blue region when excited at $\lambda_{\text{exc}} = 400 \text{ nm}$, with those containing methyl-substituted phenanthrolines having the higher quantum yield ($\approx 14\%$) in the solid state.

Supplementary Materials: The following supporting information can be downloaded at: <https://www.mdpi.com/article/10.3390/chemistry5040162/s1>: Figures S1 and S2: ¹H and ¹³C NMR spectra of the complex [Pd(η^3 -allyl)Cl]₂ in CDCl₃ at 298 K. Figures S3–S8: ¹H NMR spectra of complexes (1)–(6). Figures S9–S14: HR-ESI-MS of complexes (1)–(6). Figures S15–S17: ¹³C NMR spectra of complexes (4), (5) and (6a). Figure S18: A packing diagram of compound (6), down to the b axis of the unit cell. Hydrogen atoms of the allyl group have been omitted for clarity. Figure S19: A packing diagram of compound (6a), down to the a axis of the unit cell.

Author Contributions: A.G. (Antonia Garypidou), E.S. and D.T.: methodology, validation, investigation and editing. M.M.: investigation. K.Y. and T.T.: conceptualization, writing—original draft preparation and supervision. A.G. (Achilleas Garoufis) and J.C.P.: conceptualization, supervision, writing—review, and editing. All authors have read and agreed to the published version of the manuscript.

Funding: There was no funding for this project.

Data Availability Statement: Data are contained within the article and supplementary materials.

Acknowledgments: We acknowledge the Unit of Environmental, Organic and Biochemical high-resolution analysis-ORBITRAP-LC-MS, the X-ray Center of single crystal diffraction and the NMR Centre of the University of Ioannina for providing access to the facilities.

Conflicts of Interest: The authors declare no conflict of interest.

References

1. Zou, S.J.; Shen, Y.; Xie, F.M.; De Chen, J.; Li, Y.Q.; Tang, J.X. Recent advances in organic light-emitting diodes: Toward smart lighting and displays. *Mater. Chem. Front.* **2020**, *4*, 788–820. [CrossRef]
2. Salehi, A.; Fu, X.; Shin, D.; So, F. Recent Advances in OLED Optical Design. *Adv. Funct. Mater.* **2019**, *29*, 1808803. [CrossRef]
3. Hong, G.; Gan, X.; Leonhardt, C.; Zhang, Z.; Seibert, J.; Busch, J.M.; Bräse, S. A Brief History of OLEDs—Emitter Development and Industry Milestones. *Adv. Mater.* **2021**, *33*, 2005630. [CrossRef]
4. Bauri, J.; Choudhary, R.B.; Mandal, G. Recent advances in efficient emissive materials-based OLED applications: A review. *J. Mater. Sci.* **2021**, *56*, 18837–18866. [CrossRef]

5. Yao, B.; Giel, M.C.; Hong, Y. Detection of kidney disease biomarkers based on fluorescence technology. *Mater. Chem. Front.* **2021**, *5*, 2124–2142. [[CrossRef](#)]
6. Zhang, X.; Yao, B.; Hu, Q.; Hong, Y.; Wallace, A.; Reynolds, K.; Ramsey, C.; Maeder, A.; Reed, R.; Tang, Y. Detection of biomarkers in body fluids using bioprobes based on aggregation-induced emission fluorogens. *Mater. Chem. Front.* **2020**, *4*, 2548–2570. [[CrossRef](#)]
7. Gupta, G.; You, Y.; Hadiputra, R.; Jung, J.; Kang, D.K.; Lee, C.Y. Heterometallic bodipy-based molecular squares obtained by self-assembly: Synthesis and biological activities. *ACS Omega* **2019**, *4*, 13200–13208. [[CrossRef](#)]
8. Qi, Y.L.; Wang, H.R.; Chen, L.L.; Duan, Y.T.; Yang, S.Y.; Zhu, H.L. Recent advances in small-molecule fluorescent probes for studying ferroptosis. *Chem. Soc. Rev.* **2022**, *51*, 7752–7778. [[CrossRef](#)]
9. Pham, T.C.; Nguyen, V.-N.; Choi, Y.; Lee, S.; Yoon, J. Recent Strategies to Develop Innovative Photosensitizers for Enhanced Photodynamic Therapy. *Chem. Rev.* **2021**, *121*, 13454–13619. [[CrossRef](#)]
10. Pal, T.K. Metal-organic framework (MOF)-based fluorescence ‘turn-on’ sensors. *Mater. Chem. Front.* **2022**, *7*, 405–441. [[CrossRef](#)]
11. Tsutsui, T.; Kusaba, S.; Yamashina, M.; Akita, M.; Yoshizawa, M. Open versus Closed Polyaromatic Nanocavity: Enhanced Host Abilities toward Large Dyes and Pigments. *Chem.—A Eur. J.* **2019**, *25*, 4320–4324. [[CrossRef](#)]
12. Wu, W.; Li, Z. Nanoprobes with aggregation-induced emission for theranostics. *Mater. Chem. Front.* **2021**, *5*, 603–626. [[CrossRef](#)]
13. Lee, L.C.C.; Lo, K.K.W. Luminescent and Photofunctional Transition Metal Complexes: From Molecular Design to Diagnostic and Therapeutic Applications. *J. Am. Chem. Soc.* **2022**, *144*, 14420–14440. [[CrossRef](#)] [[PubMed](#)]
14. Dalmau, D.; Urriolabeitia, E.P. Luminescence and Palladium: The Odd Couple. *Molecules* **2023**, *28*, 2663. [[CrossRef](#)] [[PubMed](#)]
15. Yersin, H.; Rausch, A.F.; Czerwieniec, R.; Hofbeck, T.; Fischer, T. The triplet state of organo-transition metal compounds. Triplet harvesting and singlet harvesting for efficient OLEDs. *Coord. Chem. Rev.* **2011**, *255*, 2622–2652. [[CrossRef](#)]
16. Wegeberg, C.; Wenger, O.S. Luminescent First-Row Transition Metal Complexes. *JACS Au* **2021**, *1*, 1860–1876. [[CrossRef](#)]
17. Cebrián, C.; Mauro, M. Recent advances in phosphorescent platinum complexes for organic light-emitting diodes. *Beilstein J. Org. Chem.* **2018**, *14*, 1459–1481. [[CrossRef](#)] [[PubMed](#)]
18. Yang, X.; Yao, C.; Zhou, G. Highly Efficient Phosphorescent Materials Based on Platinum Complexes and Their Devices (OLEDs). *Platin. Met. Rev.* **2013**, *57*, 2–16. [[CrossRef](#)]
19. Herberger, J.; Winter, R.F. Platinum emitters with dye-based σ -aryl ligands. *Coord. Chem. Rev.* **2019**, *400*, 213048. [[CrossRef](#)]
20. Puttock, E.V.; Walden, M.T.; Williams, J.A.G. The luminescence properties of multinuclear platinum complexes. *Coord. Chem. Rev.* **2018**, *367*, 127–162. [[CrossRef](#)]
21. Sifnaiou, E.; Garypidou, A.; Ypsilantis, K.; Plakatouras, J.C.; Garoufis, A. Synthesis, characterization and photophysical properties of mixed ligand cyclometalated platinum(II) complexes containing 2-phenylpyridine and pyridine carboxylic acids. *Polyhedron* **2023**, *231*, 116252. [[CrossRef](#)]
22. Nazeeruddin, M.K.; Grätzel, M. Transition Metal Complexes for Photovoltaic and Light Emitting Applications. In *Photofunctional Transition Metal Complexes*; Springer: Berlin/Heidelberg, Germany, 2007; pp. 113–175.
23. To, W.P.; Wan, Q.; Tong, G.S.M.; Che, C.M. Recent Advances in Metal Triplet Emitters with d6, d8, and d10 Electronic Configurations. *Trends Chem.* **2020**, *2*, 796–812. [[CrossRef](#)]
24. Yang, X.; Zhou, G.; Wong, W.Y. Functionalization of phosphorescent emitters and their host materials by main-group elements for phosphorescent organic light-emitting devices. *Chem. Soc. Rev.* **2015**, *44*, 8484–8575. [[CrossRef](#)] [[PubMed](#)]
25. Evans, R.C.; Douglas, P.; Winscom, C.J. Coordination complexes exhibiting room-temperature phosphorescence: Evaluation of their suitability as triplet emitters in organic light emitting diodes. *Coord. Chem. Rev.* **2006**, *250*, 2093–2126. [[CrossRef](#)]
26. Kuwabara, J.; Ogawa, Y.; Taketoshi, A.; Kanbara, T. Enhancement of the photoluminescence of a thioamide-based pincer palladium complex in the crystalline state. *J. Organomet. Chem.* **2011**, *696*, 1289–1293. [[CrossRef](#)]
27. Laga, E.; Dalmau, D.; Arregui, S.; Crespo, O.; Jimenez, A.I.; Pop, A.; Silvestru, C.; Urriolabeitia, E.P. Fluorescent Orthopalladated Complexes of 4-Arylidene-5(4H)-oxazolones from the Kaede Protein: Synthesis and Characterization. *Molecules* **2021**, *26*, 1238. [[CrossRef](#)]
28. Expósito, J.E.; Aullón, G.; Bardají, M.; Miguel, J.A.; Espinet, P. Fluorescent perylenylpyridine complexes: An experimental and theoretical study. *Dalt. Trans.* **2020**, *49*, 13326–13338. [[CrossRef](#)]
29. Li, G.; Zheng, J.; Zhao, X.; Fleetham, T.; Yang, Y.F.; Wang, Q.; Zhan, F.; Zhang, W.; Fang, K.; Zhang, Q.; et al. Tuning the Excited State of Tetradentate Pd(II) Complexes for Highly Efficient Deep-Blue Phosphorescent Materials. *Inorg. Chem.* **2020**, *59*, 13502–13516. [[CrossRef](#)]
30. Wan, Q.; To, W.P.; Chang, X.; Che, C.M. Controlled Synthesis of PdII and PtII Supramolecular Copolymer with Sequential Multiblock and Amplified Phosphorescence. *Chem* **2020**, *6*, 945–967. [[CrossRef](#)]
31. Accorsi, G.; Listorti, A.; Yoosaf, K.; Armaroli, N. 1,10-Phenanthrolines: Versatile building blocks for luminescent molecules, materials and metal complexes. *Chem. Soc. Rev.* **2009**, *38*, 1690. [[CrossRef](#)]
32. de França, B.M.; Oliveira, S.S.C.; Souza, L.O.P.; Mello, T.P.; Santos, A.L.S.; Forero, J.S.B. Synthesis and photophysical properties of metal complexes of curcumin dyes: Solvatochromism, acidochromism, and photoactivity. *Dye. Pigment.* **2022**, *198*, 110011. [[CrossRef](#)]
33. Büyükeksi, S.I.; Şengül, A.; Erdönmez, S.; Altındal, A.; Orman, E.B.; Özkaya, A.R. Spectroscopic, electrochemical and photovoltaic properties of Pt(II) and Pd(II) complexes of a chelating 1,10-phenanthroline appended perylene diimide. *Dalt. Trans.* **2018**, *47*, 2549–2560. [[CrossRef](#)] [[PubMed](#)]

34. Ramdeehul, S.; Barloy, L.; Osborn, J.A.; De Cian, A.; Fischer, J. Synthesis, Solution Dynamics, and Crystal Structures of (2,2':6',2''-Terpyridine)(η^1 - and η^3 -allyl)palladium(II) Complexes. *Organometallics* **1996**, *15*, 5442–5444. [[CrossRef](#)]
35. Hansson, S.; Norrby, P.O.; Soegren, M.P.; Aakermark, B.; Cucciolito, M.E.; Giordano, F.; Vitagliano, A. Effects of Phenanthroline Type Ligands on the Dynamic Processes of (η^3 -Allyl) palladium Complexes. Molecular Structure of (2,9-Dimethyl-1,10-phenanthroline) [(1, 2, 3- η)-3-methyl-2-butenyl]-chloropalladium. *Organometallics* **1993**, *12*, 4940–4948. [[CrossRef](#)]
36. Sjoegren, M.; Hansson, S.; Norrby, P.O.; Aakermark, B.; Cucciolito, M.E.; Vitagliano, A. Selective stabilization of the anti isomer of (. eta. 3-allyl)palladium and -platinum complexes. *Organometallics* **1992**, *11*, 3954–3964. [[CrossRef](#)]
37. Vitagliano, A.; Aakermark, B.; Hansson, S. Convenient synthesis of cationic (. eta. 3-allyl)palladium complexes. Preparative and stereochemical aspects. *Organometallics* **1991**, *10*, 2592–2599. [[CrossRef](#)]
38. Gogoll, A.; Oernebros, J.; Grennberg, H.; Baekvall, J.-E. Mechanism of Apparent. pi.-Allyl Rotation in (. pi.-Allyl)palladium Complexes with Bidentate Nitrogen Ligands. *J. Am. Chem. Soc.* **1994**, *116*, 3631–3632. [[CrossRef](#)]
39. Parisotto, S.; Deagostino, A. π -Allylpalladium Complexes in Synthesis: An Update. *Synthesis* **2019**, *51*, 1892–1912. [[CrossRef](#)]
40. Liu, Y.; Oble, J.; Pradal, A.; Poli, G. Catalytic Domino Annulations through η^3 -Allylpalladium Chemistry: A Never-Ending Story. *Eur. J. Inorg. Chem.* **2020**, *2020*, 942–961. [[CrossRef](#)]
41. Du, J.; Li, Y.-F.; Ding, C.-H. Recent advances of Pd-p-allyl zwitterions in cycloaddition reactions. *Chinese Chem. Lett.* **2023**, *34*, 108401. [[CrossRef](#)]
42. Scattolin, T.; Pessotto, I.; Cavarzerani, E.; Canzonieri, V.; Orian, L.; Demitri, N.; Schmidt, C.; Casini, A.; Bortolamiol, E.; Visentin, F.; et al. Indenyl and Allyl Palladate Complexes Bearing N-Heterocyclic Carbene Ligands: An Easily Accessible Class of New Anticancer Drug Candidates. *Eur. J. Inorg. Chem.* **2022**, *2022*, e202200103. [[CrossRef](#)]
43. Tupini, C.; Zurlo, M.; Gasparello, J.; Lodi, I.; Finotti, A.; Scattolin, T.; Visentin, F.; Gambari, R.; Lampronti, I. Combined Treatment of Cancer Cells Using Allyl Palladium Complexes Bearing Purine-Based NHC Ligands and Molecules Targeting MicroRNAs miR-221-3p and miR-222-3p: Synergistic Effects on Apoptosis. *Pharmaceutics* **2023**, *15*, 1332. [[CrossRef](#)]
44. Scattolin, T.; Bortolamiol, E.; Visentin, F.; Palazzolo, S.; Caligiuri, I.; Perin, T.; Canzonieri, V.; Demitri, N.; Rizzolio, F.; Togni, A. Palladium(II)- η^3 -Allyl Complexes Bearing N-Trifluoromethyl N-Heterocyclic Carbenes: A New Generation of Anticancer Agents that Restrain the Growth of High-Grade Serous Ovarian Cancer Tumors. *Chem. A Eur. J.* **2020**, *26*, 11868–11876. [[CrossRef](#)] [[PubMed](#)]
45. Scattolin, T.; Bortolamiol, E.; Rizzolio, F.; Demitri, N.; Visentin, F. Allyl palladium complexes bearing carbohydrate-based N-heterocyclic carbenes: Anticancer agents for selective and potent in vitro cytotoxicity. *Appl. Organomet. Chem.* **2020**, *34*, e5876. [[CrossRef](#)]
46. Mayoral, M.J.; Ovejero, P.; Campo, J.A.; Heras, J.V.; Oliveira, E.; Pedras, B.; Lodeiro, C.; Cano, M. Exploring photophysical properties of new boron and palladium (II) complexes with β -diketone pyridine type ligands: From liquid crystals to metal fluorescence probes. *J. Mater. Chem.* **2011**, *21*, 1255–1263. [[CrossRef](#)]
47. Scattolin, T.; Andreetta, G.; Mauceri, M.; Rizzolio, F.; Demitri, N.; Canzonieri, V.; Visentin, F. Imidazo[1,5-a]pyridine-3-ylidenes and dipyrroimidazolonylidenes as ancillary ligands in Palladium allyl complexes with potent in vitro anticancer activity. *J. Organomet. Chem.* **2021**, *952*, 122014. [[CrossRef](#)]
48. Kasselouri, S.; Garoufis, A.; Katehanakis, A.; Kalkanis, G.; Perlepes, S.P.; Hadjiliadis, N. 1:1 Metal complexes of 2-(2'-pyridyl) quinoxaline, a ligand unexpectedly formed by the reaction between 2-acetylpyridine and 1,2-phenylenediamine. *Inorganica Chim. Acta* **1993**, *207*, 255–258. [[CrossRef](#)]
49. Tatsuno, Y.; Yoshida, T.; Otsuka, S.E.I.; Syntheses, I. *Inorganic Syntheses*; Wiley: Hoboken, NJ, USA, 1990.
50. APEX 3; SAINT, SHELXT; Bruker AXS Inc.: Fitchburg, WI, USA, 2016.
51. Sheldrick, G.M. SADABS; University of Göttingen: Göttingen, Germany, 1996.
52. Sheldrick, G.M. Crystal structure refinement with SHELXL. *Acta Crystallogr. Sect. C Struct. Chem.* **2015**, *71*, 3–8. [[CrossRef](#)] [[PubMed](#)]
53. Hübschle, C.B.; Sheldrick, G.M.; Dittrich, B. ShelXle: A Qt graphical user interface for SHELXL. *J. Appl. Crystallogr.* **2011**, *44*, 1281–1284. [[CrossRef](#)]
54. Spek, A.L. Structure validation in chemical crystallography. *Acta Crystallogr. Sect. D Biol. Crystallogr.* **2009**, *65*, 148–155. [[CrossRef](#)]
55. Barbour, L.J. X-Seed—A Software Tool for Supramolecular Crystallography. *J. Supramol. Chem.* **2001**, *1*, 189–191. [[CrossRef](#)]
56. Yasuda, M.; Sone, K.; Yamasaki, K. Stability of Zinc and Cadmium Complexes with Some Methyl Derivatives of 1,10-Phenanthroline and 2,2'-Bipyridine. *J. Phys. Chem.* **1956**, *60*, 1667–1668. [[CrossRef](#)]
57. Yamasaki, K.; Yasuda, M. Stability of Zinc and Cadmium Complexes with 2,2'-Bipyridine and 1,10-Phenanthroline. *J. Am. Chem. Soc.* **1956**, *78*, 1324. [[CrossRef](#)]
58. Babenko, M.; Busev, A.I.; Blokh, M.S. Extraction-spectrometric study of complexes formed during reaction of vanadium (ii), 1, 10-phenanthroline and bengal rose-a. *Zhurnal Neorg. Khimii* **1973**, *18*, 1326–1330.
59. Torralba, M.C.; Cano, M.; Campo, J.A.; Heras, J.V.; Pinilla, E.; Torres, M.R. Pyrazole-based allylpalladium complexes: Supramolecular architecture and liquid crystal behaviour. *Inorg. Chem. Commun.* **2006**, *9*, 1271–1275. [[CrossRef](#)]
60. Torralba, M.C.; Cano, M.; Campo, J.A.; Heras, J.V.; Pinilla, E.; Torres, M.R. Liquid crystal behaviour of ionic allylpalladium complexes containing 2-pyrazolopyridine as bidentate N,N'-ligand. *J. Organomet. Chem.* **2006**, *691*, 765–778. [[CrossRef](#)]

61. Amadio, E.; Scrivanti, A.; Chessa, G.; Matteoli, U.; Beghetto, V.; Bertoldini, M.; Rancan, M.; Dolmella, A.; Venzo, A.; Bertani, R. Synthesis, characterization and low temperature self assembling of (η^3 -allyl)palladium complexes with 2-pyridyl-1,2,3-triazole bidentate ligands. Study of the catalytic activity in Suzuki–Miyaura reaction. *J. Organomet. Chem.* **2012**, *716*, 193–200. [[CrossRef](#)]
62. Groom, C.R.; Bruno, I.J.; Lightfoot, M.P.; Ward, S.C. The Cambridge Structural Database. *Acta Crystallogr. Sect. B Struct. Sci. Cryst. Eng. Mater.* **2016**, *72*, 171–179. [[CrossRef](#)]
63. Böttcher, L.; Scholz, A.; Walther, D.; Weisbach, N.; Görls, H. Mononucleare Oxalamidinkomplexe von Kupfer(I), Palladium(II) und Ruthenium(II) durch gekoppelte Kation-/Anionkoordination. *Zeitschrift Anorg. Allg. Chemie* **2003**, *629*, 2103–2112. [[CrossRef](#)]
64. Wild, U.; Kaifer, E.; Himmel, H. Redox Chemistry and Group 10 Metal Complexes of Aromatic Compounds with Bulky Bicyclic Guanidino Groups. *Eur. J. Inorg. Chem.* **2011**, *2011*, 4220–4233. [[CrossRef](#)]
65. Löffler, J.; Gauld, R.M.; Feichtner, K.S.; Rodstein, I.; Zur, J.A.; Handelsmann, J.; Schwarz, C.; Gessner, V.H. Ylide-Substituted Phosphines with a Cyclic Ylide-Backbone: Angle Dependence of the Donor Strength. *Organometallics* **2021**, *40*, 2888–2900. [[CrossRef](#)] [[PubMed](#)]
66. Chan, S.C.; Chan, M.C.W.; Wang, Y.; Che, C.M.; Cheung, K.K.; Zhu, N. Organic light-emitting materials based on bis(arylacetylide)platinum(II) complexes bearing substituted bipyridine and phenanthroline ligands: Photo- and electro-luminescence from 3MLCT excited states. *Chem A Eur. J.* **2001**, *7*, 4180–4190. [[CrossRef](#)]

Disclaimer/Publisher’s Note: The statements, opinions and data contained in all publications are solely those of the individual author(s) and contributor(s) and not of MDPI and/or the editor(s). MDPI and/or the editor(s) disclaim responsibility for any injury to people or property resulting from any ideas, methods, instructions or products referred to in the content.